Optimizing densification and mechanical properties of spark plasma sintered ZrB_2-SiC ceramic composites

Krinis, Iason; Jindal, Prakhar; Popovich, Vera; Brouwer, Hans; Botchu, Jyoti; Tang, Yinglu

DOI
10.1016/j.ceramint.2025.06.408

Publication date
2025

Document Version
Final published version

Published in
Ceramics International

Ceramics International 51 (2025) 41877–41890

Contents lists available at ScienceDirect

Ceramics International

journal homepage: www.elsevier.com/locate/ceramint

Optimizing densification and mechanical properties of spark plasma sintered ZrB_2-SiC ceramic composites

Iason Krinis [a], Prakhar Jindal [b,*], Vera Popovich [a], Hans Brouwer [a], Jyoti Botchu [b], Yinglu Tang [c]

[a] Materials Science and Engineering, Faculty of Mechanical Engineering, TU Delft, Netherlands
[b] Space Systems Engineering, Faculty of Aerospace Engineering, TU Delft, Netherlands
[c] Dept. of Aerospace Structures and Materials, Faculty of Aerospace Engineering, TU Delft, Netherlands

ARTICLE INFO

Handling editor:Dr P. Vincenzini

Keywords:
Ultra-high-temperature ceramics (UHTCs)
ZrB_2-SiC
Spark plasma sintering
Densification
Mechanical properties
Milling

ABSTRACT

This study investigates the impact of different powder milling methods on the densification and mechanical properties of ZrB_2-SiC ceramic composites processed via spark plasma sintering (SPS). Powders were prepared using two ball milling techniques: tungsten carbide (WC) and conventional ZrO_2. The densification behavior during SPS was monitored, and the sintered samples were evaluated for their relative density, hardness, fracture toughness, and flexural strength. Results show that WC milling significantly enhances densification, achieving 99.2 % relative density at 2100 °C/65 MPa/15 min, compared to 96.5 % for ZrO_2-milled samples. This improvement is due to WC's sintering aid effect, which promotes grain boundary diffusion and particle packing. However, ZrO_2-milled composites exhibit superior hardness (17.38 GPa) and fracture toughness (3.97 MPa $m^{1/2}$), attributed to their refined grain structure and the absence of softer ZrO_2 phases. Conversely, WC-milled samples show slightly higher flexural strength (384–516 MPa), likely due to the transformation toughening effect of the secondary ZrO_2 phase. Overall, WC milling improves densification and flexural strength, while ZrO_2 milling yields finer-grained composites with higher hardness and toughness, making it better suited for wear-resistant and mechanically demanding applications.

1. Introduction

Space exploration and aerospace technology are rapidly evolving, driving the demand for materials capable of withstanding extreme thermal and mechanical conditions. Components such as rocket nozzles, leading edges of re-entry vehicles, and hypersonic flight surfaces are subjected to intense heat, rapid temperature fluctuations, and severe mechanical stresses. To endure these harsh environments, ceramic matrix composites (CMCs) have been widely employed due to their exceptional thermal resistance, high strength-to-weight ratio, and structural stability. Among them, carbon/carbon (C/C) and carbon/silicon carbide (C/SiC) composites have gained prominence in aerospace applications. However, their performance is limited by oxidation vulnerability. C/C composites rapidly oxidize above 500 °C without protective coatings, while C/SiC composites face active oxidation of the SiC matrix above 1650 °C, restricting their long-term usability [1]. To overcome these limitations, ultra-high temperature ceramics (UHTCs) have emerged as a promising class of materials for extreme aerospace applications. Transition metal diborides, particularly zirconium diboride (ZrB_2) and hafnium diboride (HfB_2), have attracted considerable attention due to their remarkable properties, including melting points exceeding 3000 °C, high thermal conductivity, and excellent oxidation and wear resistance [2]. Among these, ZrB_2 is especially preferred for aerospace applications due to its lower density, reduced cost, and superior thermal shock resistance compared to HfB_2, making it a viable candidate for reusable rocket nozzle liners and thermal protection systems [3].

However, despite its outstanding thermal stability, monolithic ZrB_2 suffers from intrinsic brittleness, low fracture toughness, and limited oxidation resistance, which hinder its structural applications under severe conditions [4–6]. To address these limitations, silicon carbide (SiC) is frequently incorporated as a secondary phase, creating ZrB_2-SiC composites with significantly improved properties. The addition of SiC enhances the oxidation resistance of ZrB_2 by forming a protective silica (SiO_2) layer during high-temperature exposure, preventing further degradation. Moreover, SiC reinforcement increases the hardness,

* Corresponding author.
E-mail address: p.jindal@tudelft.nl (P. Jindal).

https://doi.org/10.1016/j.ceramint.2025.06.408
Received 3 April 2025; Received in revised form 5 June 2025; Accepted 26 June 2025
Available online 28 June 2025

flexural strength, and fracture toughness of the composite by promoting grain refinement and crack deflection mechanisms. Studies have demonstrated that 20 vol% SiC offers an optimal balance, enhancing oxidation resistance up to 1600 °C, boosting hardness, and improving mechanical reliability [7]. To effectively consolidate ZrB_2-SiC composites, spark plasma sintering (SPS) has emerged as a highly efficient densification technique. SPS offers several advantages over conventional sintering methods, including lower sintering temperatures, faster densification rates, and limited grain growth. The application of pulsed DC current and uniaxial pressure during SPS accelerates mass transport, enabling the production of dense composites with refined microstructures and enhanced mechanical properties [8].

The pre-sintering preparation of ZrB_2-SiC powders plays a pivotal role in determining the final properties of the composites. Achieving a homogeneous dispersion of the ZrB_2 and SiC phases is critical for obtaining consistent mechanical performance. Two primary methods are commonly used for powder preparation: conventional mixing and high-energy milling. Conventional mixing typically results in larger, less uniform particles, leading to lower sinterability and reduced mechanical performance. In contrast, high-energy milling promotes finer particle sizes, better mixing homogeneity, and increased surface activation, all of which enhance the sintering kinetics. Furthermore, the choice of milling media significantly influences the powder characteristics. Zirconia (ZrO_2) and tungsten carbide (WC) balls are widely used due to their high density and wear resistance. However, they introduce distinct effects on the composite's properties. WC media can act as a sintering aid, enhancing grain boundary diffusion and promoting densification, while ZrO_2 balls produce minimal contamination, leading to purer composites with more consistent mechanical properties. Despite the growing interest in ZrB_2-SiC UHTCMCs, the impact of powder mixing methods and milling media on their densification behavior, microstructure evolution, and mechanical properties remains insufficiently explored. Previous studies have primarily focused on the sintering conditions and oxidation resistance, with limited attention given to the influence of powder preparation techniques on the final composite performance.

This study addresses a critical gap by systematically investigating the influence of milling methods and media on the densification, microstructure, and mechanical performance of spark plasma sintered ZrB_2-SiC composites. By comparing high-energy WC milling with conventional ZrO_2 milling, this work provides new insights into how the sintering aid effect of WC enhances densification while ZrO_2 milling produces finer-grained composites with superior hardness and fracture toughness. The findings offer valuable guidelines for optimizing powder preparation strategies, enabling the design of UHTCMCs with tailored properties for next-generation aerospace applications, including reusable rocket nozzles, thermal protection systems, and hypersonic vehicles.

2. Materials and methods

2.1. Preparation and sintering of ZrB_2-SiC composites

2.1.1. Raw materials

Zirconium Diboride (ZrB_2) and Silicon Carbide (SiC) powders were utilized as primary raw materials for fabricating ultra-high-temperature ceramic matrix composites. ZrB_2 powder (hexagonal crystal phase) was sourced with a purity of 99.5 % (Zr: 80 %, B: 18.90 %, N: 0.08 %, Si: 0.1 %), a density of 6.09 g/cm^3, and an average particle size of 5.5 μm. SiC powder (beta-phase) had a purity of 99.8 % metals basis (free C: 1.33 %, O: 0.57 %, Fe: 151 ppm, Al: 20 ppm, Ca: 10 ppm), with a density of 3.21 g/cm^3 and an average particle size of 0.62 μm. The powders were mixed to maintain a ZrB_2:SiC volume ratio of 80:20, optimizing mechanical strength and oxidation resistance for aerospace applications.

2.1.2. Powder milling techniques

Two distinct milling techniques were employed to prepare the ceramic composite powders, evaluating the impact of milling media and processing parameters on the final microstructure and mechanical properties of the sintered samples. For ZrO_2-milled samples (ZSZ), ZrB_2 and SiC powders were ball-mixed in a glass beaker for 48 h using 10 mm diameter zirconia (ZrO_2) balls and ethanol as the grinding liquid. Continuous rolling motion at room temperature ensured thorough mixing and particle refinement. Post-mixing, the powders were dried at 180 °C for 12 h to evaporate ethanol and prevent agglomeration, then sieved through a 100 μm mesh for uniform particle size distribution. For WC-milled samples (ZSW), high-energy ball milling was performed in a WC-lined jar at 300 rpm for 10 h using 5 mm diameter pure tungsten carbide (WC) balls and isopropyl alcohol (IPA) as the milling liquid. Shorter milling duration and higher rotational speed enhanced mixing homogeneity while minimizing contamination from WC media. The preparation steps, including durations and media, were selected based on protocols reported in previous studies with similar procedures and demonstrated optimal properties [9–11]. Post-milling, milled powders were dried at 180 °C for 12 h and sieved through a 100 μm mesh for uniformity before sintering.

2.1.3. Spark plasma sintering (SPS) procedure

The mixed and dried ZrB_2-SiC powders were consolidated using spark plasma sintering (SPS) at TU Delft, Netherlands, utilizing an FCT Systeme GmbH SPS system. The sintering process involved loading powders into a 30 mm diameter graphite die with graphite punches at both ends. A 0.5 mm thick graphite sheet was inserted between the raw material and the die to facilitate easy extraction post-densification. The graphite die assembly was wrapped with carbon blankets to minimize heat loss and ensure uniform temperature distribution. The sintering cycle, as shown in Fig. 1, involved a heating rate of 100 °C/min, with samples held at target sintering temperatures (1950°C-2100 °C) and pressures (50–65 MPa) for 15 and 60 min in an argon (Ar) atmosphere. Pulsed DC during SPS promoted rapid densification by activating mass transport mechanisms such as diffusion and particle rearrangement, limiting grain growth and enhancing mechanical properties.

The powders were sintered to obtain a ZrB_2-SiC ceramic disc of

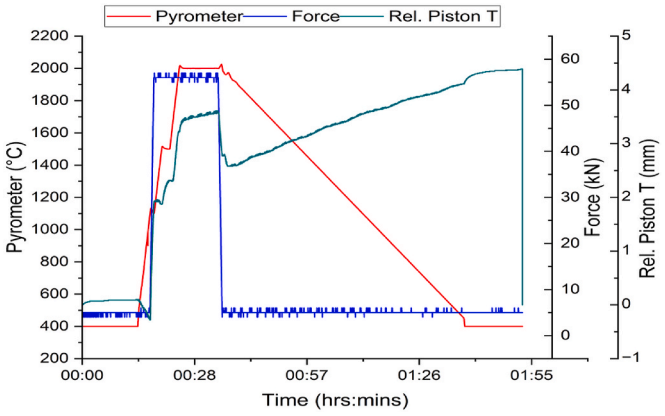

Fig. 1. Sintering cycle for the manufacture of one of the ZrB2-SiC ceramics.

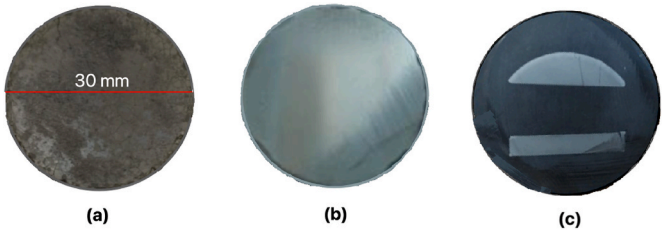

Fig. 2. ZrB_2-SiC Sample, (a) post-sintering, (b) polished and grinded sample, (c) final ceramic sample.

diameter 30 mm and 4 mm thickness, as shown in Fig. 2(a). Post-sintering, samples were polished to a mirror finish using diamond suspensions and thoroughly cleaned, as shown in Fig. 2(b). For obtaining mechanical properties and morphological results, the ceramics were first cut into desired dimensions and cast in non-conductive resin. For the final sample, before undergoing testing, a 4000-grit paper was used to grind and then polished with velvet to give a mirror-like finish, as shown in Fig. 2(c).

2.1.4. Density measurement

The relative density of the sintered ZrB_2-SiC composites was measured using Archimedes' principle, following the ASTM C373-88 standard. The polished and dried samples were weighed in air and then in distilled water as the immersion medium. The relative density (ρ) was calculated using the following formula (eq. (1)):

$$\rho = \frac{W_{air}}{W_{air} - W_{water}} \times \rho_{water} \quad (1)$$

where W_{air} = Sample weight in air; W_{water} = Sample weight in water; ρ_{water} = Density of water at the measurement temperature.

2.2. Microstructural and mechanical characterization

The microstructural characterization of the sintered ZrB_2-SiC composites was carried out using various techniques. Optical Microscopy (OM) was performed with a Keyence VHX-5000 digital microscope to examine the surface morphology and identify any visible defects or porosity. Scanning Electron Microscopy (SEM) was utilized to further analyze the microstructure, grain size, and phase distribution using a Jeol JSM IT-100 SEM, operated at 15 kV with both secondary electron and backscattered electron imaging modes. Image analysis was conducted using ImageJ2 software to measure the average SiC grain size based on the linear intercept method.

Phase identification was performed using X-ray diffraction (XRD) to identify the crystalline phases and detect any secondary phases resulting from the milling media interaction. The XRD analysis was conducted with a Bruker D8 Advance diffractometer, employing a Bragg-Brentano geometry, Cu-Kα radiation, a beam size of 0.5 mm diameter, and a Lynxeye XET position-sensitive detector in high-resolution mode. XRD measurements were taken on both the surface and the thickness direction of the samples to ensure comprehensive phase identification. The samples were mounted on Si510 wafers to minimize diffraction interference from the mounting surface.

The mechanical properties of the sintered samples were evaluated through hardness, flexural strength, and fracture toughness measurements. Vickers hardness was measured following the ASTM C1327-08 standard using a DuraScan 20 (Struers) hardness tester with a 1 kgf load, 15-s dwell time, and five indentations on each sample (both in-plane and through the thickness). The average hardness was calculated and expressed in GPa.

Flexural strength was measured using the 4-point bending test according to the ASTM C1161-13 standard. The test setup included a Zwick Z010 machine with an outer support span of 20 mm, an inner loading span of 10 mm, and a loading rate of 0.2 mm/min. Five sample bars were tested for each batch, and the average flexural strength was calculated using the following formula (eq.(2)):

$$\sigma_f = \frac{3PL}{4bd^2} \quad (2)$$

where P = Breaking force (N); L = Outer support span (mm); b = Width of the sample bar (mm); d = Thickness of the sample bar (mm).

The fracture toughness (K_{IC}) of the samples was estimated using the Vickers indentation method, based on the Halfpenny model for c/a >2. Five indentations were made at different locations on the sample surfaces. The formula used was (eq.(3)):

$$K_{IC} = 0.0101 \frac{P}{a\, c^{\frac{1}{2}}} \quad (3)$$

where P = Indentation load (N); a = Half the indent diagonal (mm); c = Average crack length (mm).

While the Vickers indentation method provides a convenient estimation of fracture toughness, it is not entirely reliable for brittle ceramics due to irregular crack propagation, as highlighted in prior studies [12–15]. Therefore, the results should be interpreted cautiously.

3. Results and discussion

3.1. Densification behavior of ZrB_2-SiC composites

Table 1 presents a comprehensive summary of the densification behavior and mechanical properties of all the tested ZrB_2-SiC composite samples, highlighting the influence of the milling method and sintering protocol. The samples prepared using WC ball milling (ZSW) consistently exhibited higher relative densities compared to those prepared using ZrO_2 milling (ZSZ) under similar sintering conditions.

The results demonstrate that the WC-milled samples (ZSW) consistently achieve higher relative densities than the ZrO_2-milled samples (ZSZ) across all sintering conditions. The relative density of the ZSW samples ranges from 94.7 % to a peak value of 99.2 % at 2100 °C/65 MPa/15 min (ZSW.5), as can be seen in Fig. 3, whereas the ZSZ samples achieve a lower maximum density of 96.7 % under the same conditions (ZSZ.7). The superior densification of the ZSW samples can be attributed to the sintering aid potential of tungsten carbide (WC), which enhances grain boundary diffusion and promotes more efficient particle rearrangement during SPS [16]. Furthermore, while WC contamination has been observed in other studies due to mixing [17], this was not the case in the current study. XRD analysis and SEM-EDS analysis confirmed the absence of such contamination, ensuring that the observed porosity is solely attributed to the material's relative density. WC milling also results in finer and more homogeneously distributed particles, which further improves packing efficiency and reduces the formation of voids during sintering. In contrast, while ZrO_2 milling is still effective for densification, it offers a slightly lower sintering aid effect compared to WC. This is likely due to the lower hardness and density of ZrO_2, which

Table 1
Densification and mechanical properties of all the tested samples, highlighting the influence of the milling method and sintering protocol.

SPS-protocol (°C/MPa/min)	Sample number	Relative density (%)		Avg. SiC grain size (μm)		Vickers Hardness HV1 (GPa)		Flexural Strength σ_f (MPa)		Fracture Toughness K_{IC} (MPa·m$^{1/2}$)	
		ZSW	ZSZ	ZSW	ZSZ	ZSW	ZSZ	ZSW	ZSZ	ZSW	ZSZ
1950/50/15	1	94.7	96.0	2.91	2.65	14.33	17.08	407	343	3.71	3.97
2050/50/15	2	97.7	96.2	–	–	13.92	15.76	384	317	3.58	3.48
2000/65/15	3	96.6	95.3	4.23	3.36	13.20	16.03	490	476	3.76	3.67
2050/65/15	4	97.1	95.9	–	–	13.92	15.98	461	434	3.55	3.78
2100/65/15	5	99.2	96.5	5.28	4.23	13.64	13.92	407	423	3.62	3.71
2000/65/60	6	97.8	96.0	–	–	15.11	15.09	516	447	3.75	3.72
2100/65/60	7	99.0	96.7	–	–	13.73	15.01	497	431	3.51	3.62

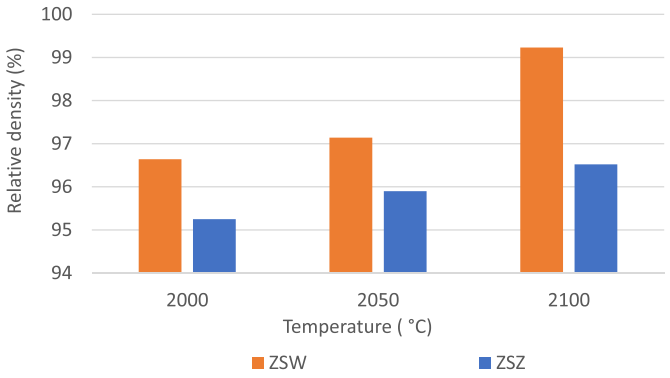

Fig. 3. Comparison of relative densities between samples fabricated using high-energy WC milling and regular ZrO_2 milling, evaluated at 65 MPa and a dwell time of 15 min across various temperatures.

results in less aggressive particle refinement during milling.

To further assess the densification behavior, X-ray diffraction (XRD) analysis was conducted on both ZSW and ZSZ samples to determine phase composition and identify any secondary phases introduced during the milling and sintering processes. The analysis revealed that ZSW samples, prepared through WC ball milling, consistently exhibited the formation of a secondary ZrO_2 phase. In contrast, the ZSZ samples, milled with ZrO_2 balls, showed no evidence of secondary phase formation, indicating a cleaner and more phase-pure microstructure. The appearance of the secondary ZrO_2 phase in the ZSW samples is likely due to contamination during high-energy milling. The increased abrasion of the WC balls and the aggressive nature of high-energy milling, combined with localized heating and potential oxidation, lead to the incorporation of ZrO_2 into the composite. This is further supported by the XRD patterns shown in Fig. 4, where distinct peaks corresponding to ZrO_2 are clearly visible in the ZSW samples.

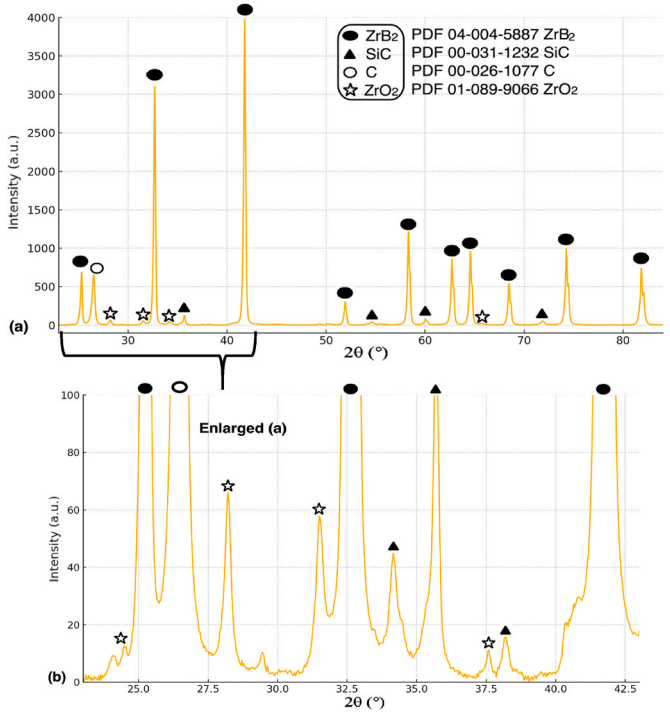

Fig. 4. XRD analysis of sample ZSW.3 (2000 °C/65 MPa/15 min) showing the formation of ZrO_2. a) Overview of the diffraction pattern, indicating phase composition; b) Magnified view, detailing the specific peaks associated with ZrO_2.

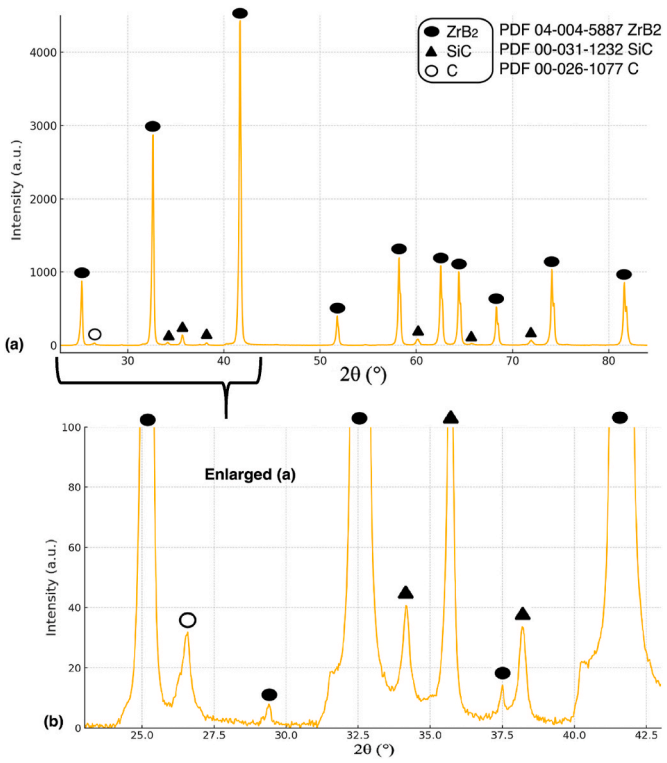

Fig. 5. XRD analysis of sample ZSZ.3 (2000 °C/65 MPa/15 min), showing no detectable formation of the ZrO_2 phase. (a) Overview of the diffraction pattern illustrating phase composition; (b) Magnified view, detailing the specific peaks, confirming the absence of ZrO_2 peaks.

Conversely, the XRD analysis of the ZSZ samples (Fig. 5) confirms the absence of any secondary ZrO_2 phase. The stability of the ZrO_2 milling balls, coupled with the less aggressive milling conditions, prevents contamination, resulting in a purer phase composition. This stability is essential for achieving cleaner phase retention and more reliable sintering behavior.

Additionally, in both milling methods, an additional carbon phase was detected, which is likely due to carbon diffusion or reaction from the graphite molds and protective graphite sheets used during high-temperature sintering.

Semi-quantitative phase analysis was conducted using Rietveld refinement on selected sintered samples (ZSW.3–ZSW.7 and ZSZ.3–ZSZ.7) to estimate the phase fractions of ZrB_2, SiC, ZrO_2, and residual carbon. XRD data were acquired over a 2θ range of 20–90°, step size 0.033° 2θ, counting time per step 2 s, using Cu-Kα radiation and refined using Bruker software DiffracSuite.EVA vs 7.1. The refinement included background correction, peak shape fitting, and scale factor optimization. As seen from Table 2, the results confirm that WC-milled samples contain 1–4 wt% monoclinic ZrO_2, absent in ZrO_2-milled

Table 2
Phase composition of selected ZSW and ZSZ samples determined by Rietveld refinement.

Sample ID	Milling Method	ZrB_2 (wt %)	SiC (wt %)	ZrO_2 (wt %)	Carbon (wt %)
ZSW.3	WC	87 %	9 %	4 %	–
ZSW.5	WC	84 %	13 %	2 %	1 %
ZSW.6	WC	82 %	13 %	4 %	2 %
ZSW.7	WC	84 %	13 %	1 %	2 %
ZSZ.3	ZrO_2	84 %	14 %	–	2 %
ZSZ.5	ZrO_2	84 %	15 %	–	1 %
ZSZ.6	ZrO_2	82 %	14 %	–	3 %
ZSZ.7	ZrO_2	83 %	15 %	–	1 %

Table 3
Effect of the ZrO_2 volume fraction on the relative density measurement of the ZSW samples.

Sample name	ρ_{exp} (g/cm^3)	ρ_t without ZrO_2(g/cm^3)	ρ_{rel} without ZrO_2 (%)	ZrO_2 vol fraction(%)	ρ_t with ZrO_2(g/cm^3)	ρ_{rel} with ZrO_2 (%)	Difference in ρ_{rel} (%)
ZSW.3	5.32	5.51	96.6	3.9	5.50	96.8	0.2
ZSW.5	5.47	5.51	99.2	1.9	5.51	99.3	0.1
ZSW.6	5.39	5.51	97.8	3.8	5.50	98.0	0.2
ZSW.7	5.45	5.51	99.0	1.0	5.51	99.0	<0.1

samples, supporting the presence of milling-induced contamination.

To evaluate the effect of the ZrO_2 secondary phase on the densification behavior of the ZSW samples, a sensitivity analysis was conducted. The volume fractions of ZrO_2 formed during the milling process were calculated using the XRD data. These values were then factored into the theoretical density calculations of the ZSW samples, considering the theoretical density of monoclinic ZrO_2 (5.68 g/cm^3). The sensitivity analysis results, presented in Table 3, show the theoretical and relative densities of the ZSW samples, both with and without accounting for the ZrO_2 phase. The analysis indicates that the impact of the secondary ZrO_2 phase on the final relative density is minimal, with the difference being less than 0.2 % across all tested samples. This suggests that the formation of the secondary phase does not significantly affect the overall densification trends.

The sensitivity analysis reveals that the presence of the ZrO_2 secondary phase has a negligible impact on the overall densification of the ZSW samples. The relative density difference between the ZrO_2-included and ZrO_2-free models is less than 0.2 %, which is within the experimental margin of error for density measurements.

This indicates that while the secondary phase formation is detectable by XRD, it does not significantly alter the densification performance of the ZSW samples. This minimal impact can be attributed to the relatively low volume fraction of ZrO_2 (ranging between 1.0 % and 3.9 %), which is insufficient to substantially influence the overall material density. Additionally, the negligible effect on densification highlights the high sinterability of the ZSW samples, even in the presence of trace secondary phases. This finding is particularly relevant for industrial applications, as it suggests that WC-milled ZrB_2-SiC composites can achieve near-theoretical densities despite minor contamination from ZrO_2, making the milling method suitable for large-scale production.

3.2. Microstructural characterization

The microstructures of the sintered ZSW and ZSZ samples were analyzed using optical microscopy at magnifications up to 2000× to evaluate the morphology, grain size, and surface features. Figs. 6 and 7 show representative microstructures of a ZSW.7 and ZSZ.7 samples, respectively, captured at 1000x (100 μm) and 1500x (50 μm) magnifications. In the optical micrographs, the light-gray/white regions correspond to the ZrB_2 matrix phase, while the dark-gray grains represent SiC

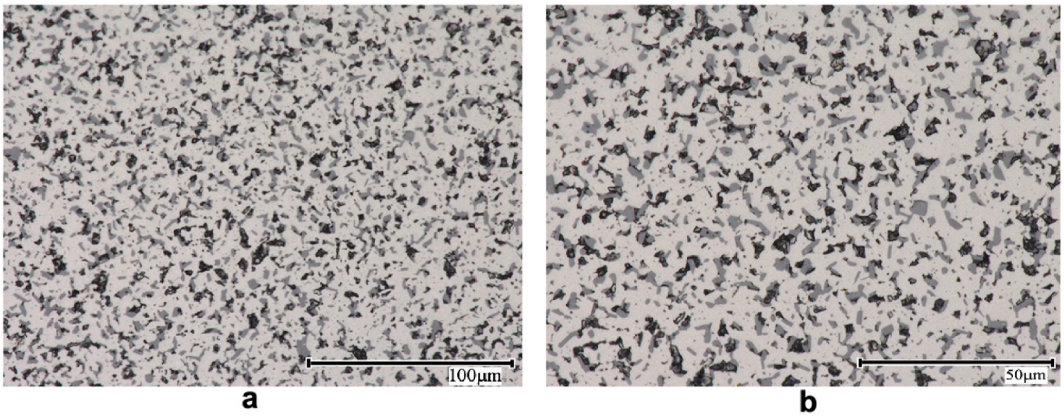

Fig. 6. Microstructure of sample ZSW.7, for different magnifications: a) x1000, b) x 1500.

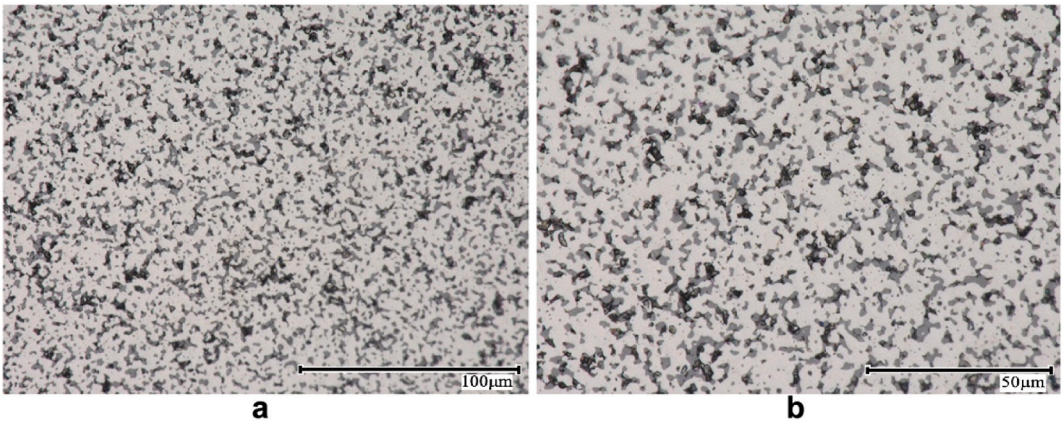

Fig. 7. Microstructure of sample ZSZ.7, for different magnifications: a) x1000, b) x1500.

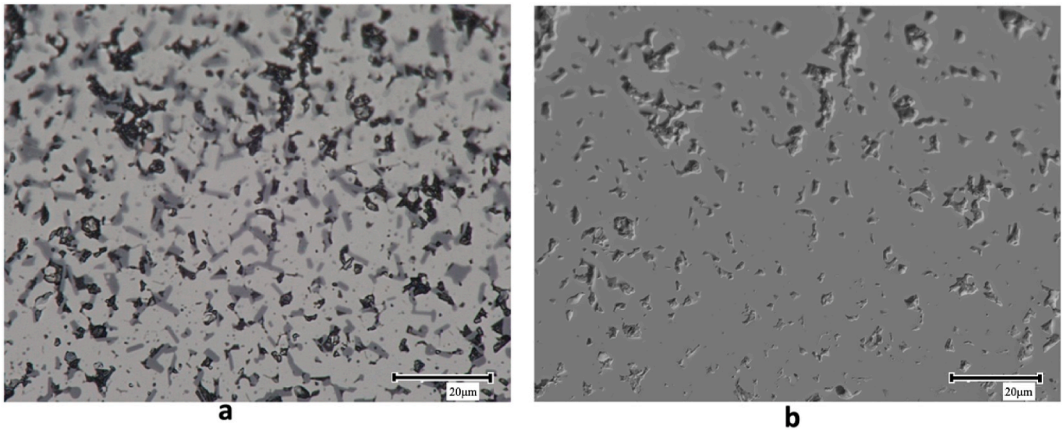

Fig. 8. a) Microstructure of sample ZSW.5, displaying grain pull-out regions and surface cavities. b) Texture analysis via optical microscope, highlighting regions with protruding bumps and cavities caused by grain pull-out.

particles. The black spots scattered across the surface indicate grain pull-out regions, which occur due to localized mechanical stress during the sintering or polishing process. The micrographs of the remaining samples are included in the appendix for reference.

Grain pull-out was observed in all samples, which is consistent with the findings reported in the literature [18]. The ZSW samples, however, exhibited more pronounced grain pull-out compared to the ZSZ samples. This disparity can be attributed to the aggressive nature of high-energy WC ball milling. During the milling process, the intense mechanical forces induce microstructural defects and weaken the grain boundaries, making the ZSW samples more susceptible to pull-out during sintering and mechanical testing. In contrast, the ZSZ samples, prepared using ZrO_2 ball milling, displayed less grain pull-out, suggesting that the milder milling conditions resulted in stronger grain boundaries and a more stable microstructure. The reduced grain pull-out in the ZSZ samples is also indicative of a more homogeneous microstructure and potentially improved mechanical properties, as fewer surface defects generally lead to enhanced strength and toughness.

To further investigate the surface characteristics, topographic surface analysis of the samples was conducted using optical microscopy. Fig. 8 displays the microstructure of sample ZSW.5, along with the texture analysis. The image reveals two distinct surface features: Cavities caused by grain pull-out (recessed regions) & Protruding bumps, representing regions where grains resisted dislodgement during polishing.

The surface roughness and the prevalence of pull-out regions were found to be slightly higher in the ZSW samples, consistent with the more intense milling process. This indicates that WC milling introduces greater surface heterogeneity, which may affect the wear resistance and mechanical stability of the material.

Fig. 8 displays the topographic surface analysis of a sample, conducted using optical microscopy, where certain regions of grain pull-out form cavities (recessed into the material surface), while other areas exhibit bumps (protruding from the material surface).

To examine the influence of the milling method and sintering parameters on the grain morphology, the average SiC grain size of selected samples was measured. Due to the anisotropic grain growth and the wide distribution of grain sizes, accurately quantifying the average grain size for these specimens was challenging. Additionally, grain pull-out during sample preparation (polishing) may have introduced minor inconsistencies in the measurements. Consequently, the standard deviations are relatively high, indicating significant variability in the grain size distribution.

As shown in Fig. 9, ZSW samples exhibit larger average grain sizes than the ZSZ samples under identical sintering conditions. The grain size increases with rising sintering temperatures and pressures. The ZSW samples exhibit coarser grains due to the more aggressive WC milling, which introduces higher defect densities, promoting grain growth during sintering.

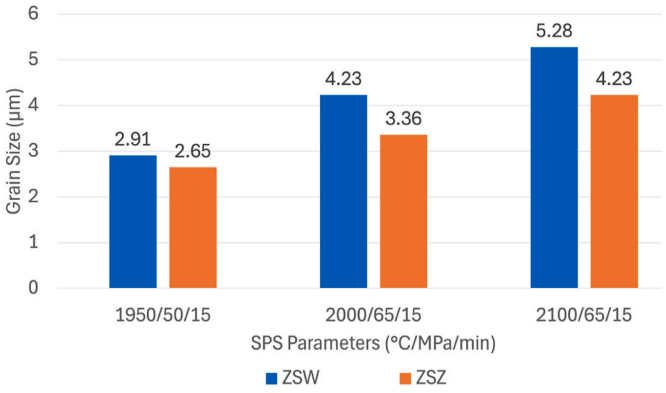

Fig. 9. Average SiC grain size during different sintering parameters for selected samples, highlighting the effects of milling method and sintering conditions.

The grain size differences are further illustrated in Fig. 10, which shows the grain size variation with the standard deviation as error bars between ZSW and ZSZ samples at different temperatures. The data reveal that higher sintering temperatures and pressures promote more significant grain coarsening due to enhanced atomic diffusion and grain boundary mobility. This phenomenon aligns with findings reported in

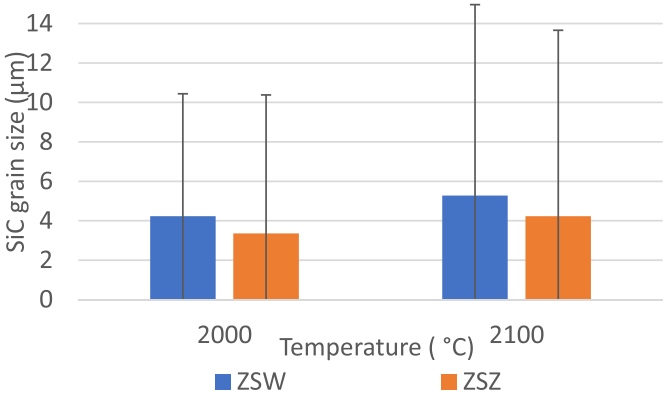

Fig. 10. Comparison of SiC grain size between ZSW and ZSZ samples at varying temperatures showing larger grains in the ZSW samples due to the more aggressive milling process.

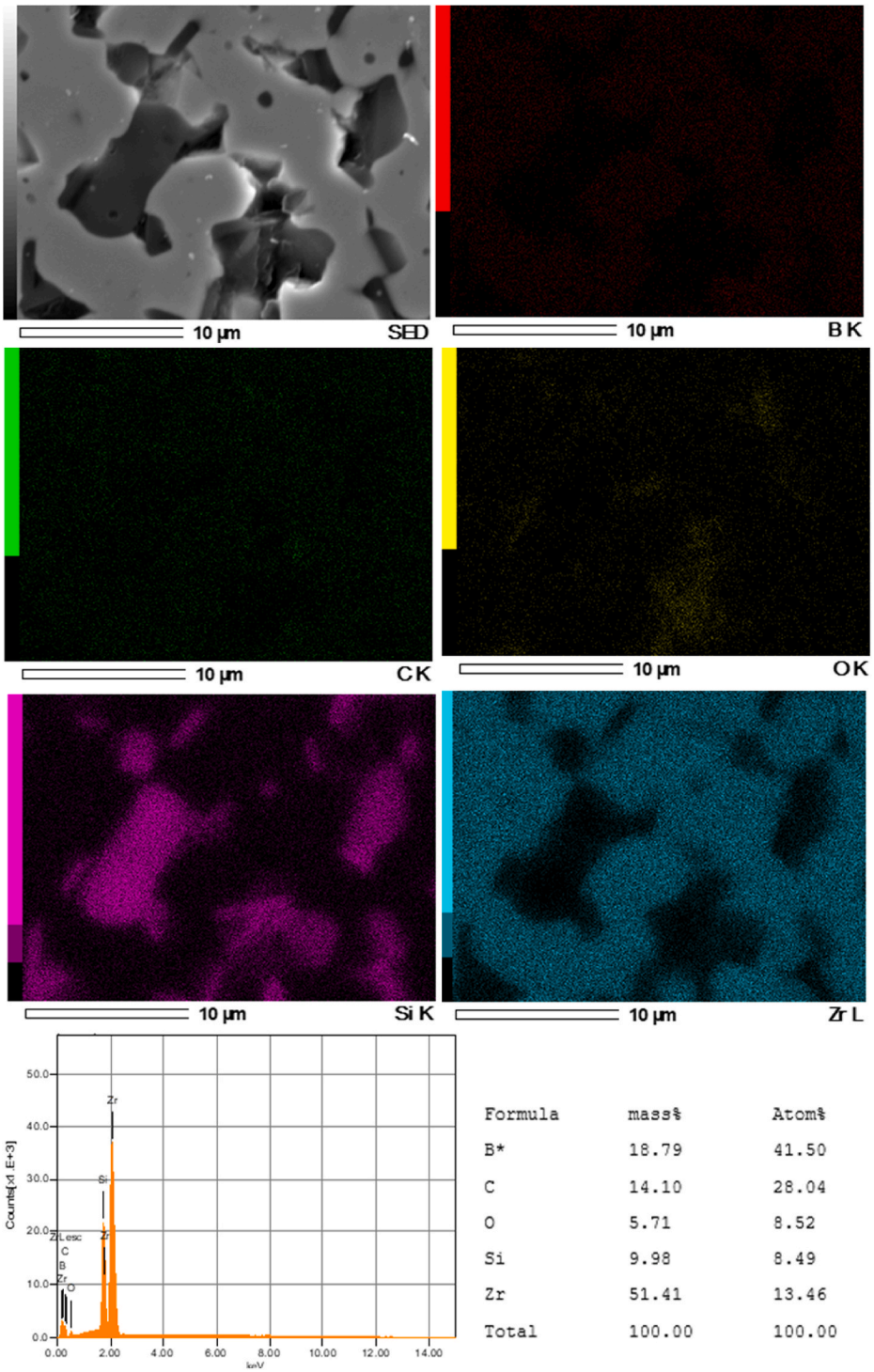

Fig. 11. SEM image and EDS analysis for sample ZSW.6, showing larger SiC grains and higher oxygen content due to ZrO_2 formation.

the literature, which attribute grain growth at elevated temperatures to the reduction in grain boundary energy. As smaller grains tend to have higher boundary energy, they are more prone to atomic diffusion, merging into larger grains. This process reduces the overall grain boundary area, resulting in a coarsened microstructure, as described in previous studies [19,20].

To further investigate the microstructural characteristics and chemical composition, SEM and EDS analyses were performed. Figs. 11 and 12 display the SEM images along with the EDS spectra (chemical analysis and composition) for the ZSW and ZSZ samples, both sintered under identical conditions. From the two figures, the presence of grain pull-out (visible as dark black cavities along the SiC grain edges) is also evident, consistent with the observations from optical microscopy. Additionally, the SiC grains appear larger in the ZSW sample compared to the ZSZ sample, and the oxygen content is higher in the ZSW. However, it should be noted that EDS measurements of light elements such as B (as also indicated by the asterisk (*) in Figs. 11 and 12), and C or O are subject to greater uncertainty, particularly at high accelerating voltages, and the reported values may carry a significant margin of error.

More specifically, the oxygen mass percentage as measured in

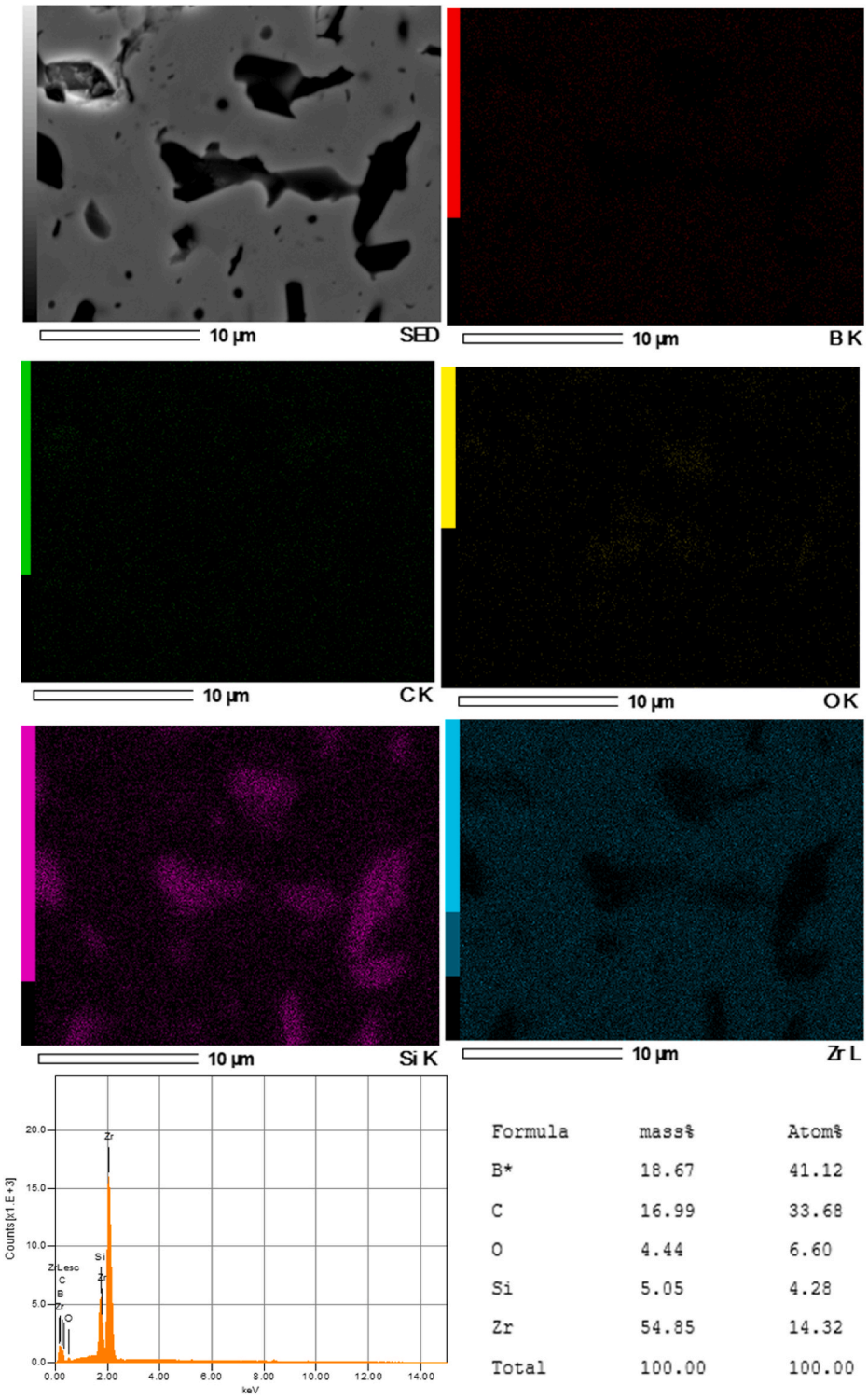

Formula	mass%	Atom%
B*	18.67	41.12
C	16.99	33.68
O	4.44	6.60
Si	5.05	4.28
Zr	54.85	14.32
Total	100.00	100.00

Fig. 12. SEM image and EDS analysis for sample ZSZ.6, displaying finer grains and lower oxygen content, indicating a more phase-pure microstructure.

sample ZSW.6, as seen in Fig. 11, was 5.71 %, compared to respective percentage measured in sample ZSZ.6, which was 4.44 %, as seen in Fig. 12. This increased oxygen concentration may be attributed to the formation of ZrO_2, as supported by the XRD results, and the more pronounced effect of grain pull-out, with greater accumulation in cavities, as shown in Fig. 11.

3.3. Mechanical properties analysis

3.3.1. Hardness

The hardness of the sintered ZrB_2-20 vol% SiC samples was evaluated to determine the impact of the milling method and sintering parameters on the material's mechanical performance. The results reveal that the ZSZ samples, produced using ZrO_2 ball milling, consistently exhibited higher hardness values compared to the ZSW samples, which were

Table 4
Average hardness values and standard deviation for ZSW and ZSZ samples, along with the corresponding sintering parameters.

SPS-protocol (°C/MPa/min)	Sample name	HV1 Average (GPa)	HV1 Standard deviation (GPa)	Sample name	HV1 Average (GPa)	HV1 Standard deviation (GPa)
1950/50/15	**ZSW.1**	14.33	0.93	**ZSZ.1**	17.08	0.25
2050/50/15	**ZSW.2**	13.92	0.40	**ZSZ.2**	15.76	0.64
2000/65/15	**ZSW.3**	13.20	0.45	**ZSZ.3**	16.03	0.24
2050/65/15	**ZSW.4**	13.92	0.26	**ZSZ.4**	15.98	0.44
2100/65/15	**ZSW.5**	13.64	0.36	**ZSZ.5**	13.92	0.33
2000/65/60	**ZSW.6**	15.11	0.48	**ZSZ.6**	15.09	0.35
2100/65/60	**ZSW.7**	13.73	0.38	**ZSZ.7**	15.01	0.45

prepared using the more aggressive WC ball milling technique. The highest average hardness was observed in ZSZ.1, sintered at 1950 °C, 50 MPa, and a dwell time of 15 min, reaching 17.08 GPa, with a relatively low standard deviation of 0.25 GPa, indicating uniformity in the microstructure.

In contrast, the ZSW sample processed under the same sintering conditions (ZSW.1) achieved a significantly lower hardness of 14.33 GPa with a higher standard deviation of 0.93 GPa, suggesting greater variability and potential microstructural inconsistencies. Table 4 summarizes the average Vickers hardness (HV1) values and the corresponding standard deviations for the ZSW and ZSZ samples under different sintering conditions.

The difference in hardness between the ZSZ and ZSW samples can be primarily attributed to the formation of the ZrO_2 secondary phase in the ZSW samples. Although the presence of ZrO_2 does not drastically influence the densification process, it notably reduces the hardness of the ZSW samples due to its relatively lower intrinsic hardness. ZrO_2 typically exhibits a Vickers hardness of 12–16 GPa (averaging around 14 GPa) [21,22], which is considerably lower than that of the ZrB_2 matrix phase (23 GPa [7]) and the SiC reinforcement phase, which can reach 24–26 GPa [23] and even up to 32 GPa in some cases [24]. The introduction of ZrO_2 into the microstructure introduces weak points, reducing the material's overall ability to resist fracture under load. Additionally, the formation of ZrO_2 disrupts the grain boundary integrity, impeding effective load transfer and making the material more prone to crack initiation and propagation under applied stress. Although the ZSW samples exhibited improved densification, their mechanical properties were notably compromised due to the presence of ZrO_2, a phenomenon that has been reported in the literature [9]. Fig. 13 illustrates the variation in hardness between ZSW and ZSZ samples as a function of sintering temperature. The plot clearly shows that ZSZ samples exhibit superior hardness across the temperature range, with a consistent 2–3 GPa advantage over the ZSW samples.

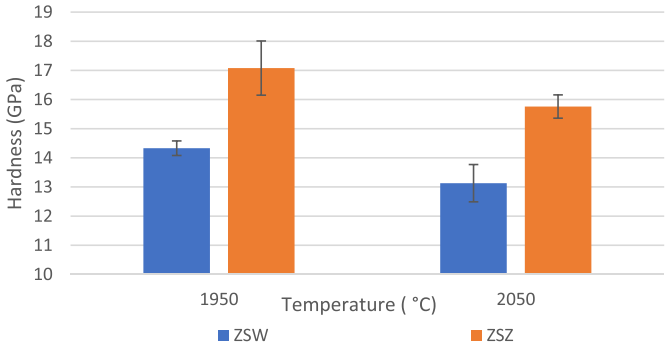

Fig. 13. Comparison of hardness values (HV1) between samples fabricated using high-energy WC milling and regular ZrO_2 milling, evaluated at 50 MPa and a dwell time of 15 min across different temperatures.

The hardness values obtained in this study are in agreement with those reported in the literature. The ZSW and ZSZ samples exhibited hardness values ranging from 13.20 to 15.11 GPa and 13.92–17.08 GPa, respectively. These results align with the findings of Naughton-Duszova et al. [2], who reported values between 15.4 and 17.9 GPa for ZrB_2-SiC composites sintered under similar conditions. Additionally, Guo et al. [9] observed hardness values ranging from 15.59 to 17.98 GPa, while Yuan et al. [18] reported an average hardness of 14.2 GPa for ZrB_2-20 vol% SiC composites. The slight variations in the hardness values between this study and previous works can be attributed to several factors, including, sintering protocol variations (temperature, pressure, and dwell time), differences in powder quality and grain size distribution, divergent testing methods and indentation parameters, variations in milling techniques, which significantly influence the microstructure and phase composition.

3.3.2. *Flexural strength*

The flexural strength of the sintered ZrB_2-SiC composites was evaluated to determine their ability to withstand bending forces and assess the impact of the milling method and sintering parameters on the material's structural integrity. As previously noted, the ZSZ samples, which feature a finer grain structure and lack the secondary ZrO_2 phase, generally demonstrate superior hardness compared to the ZSW samples. This is because finer grains create a denser, more refined microstructure, which enhances resistance to crack initiation and propagation. However, despite the lower hardness of the ZSW samples, they exhibit comparable or even slightly superior flexural strength to the ZSZ samples, as shown in Table 5 and Fig. 14. This result can be attributed to the transformation toughening mechanism of the ZrO_2 phase in the ZSW samples. When subjected to mechanical stress, the tetragonal ZrO_2 phase undergoes a stress-induced phase transformation into monoclinic ZrO_2. This transformation is accompanied by a 4–5 % volume expansion, which generates compressive stresses at the crack tip, thereby increasing the material's resistance to bending and slowing down crack propagation [25]. This energy-absorbing mechanism improves the overall flexural strength of the ZSW samples, effectively compensating for their lower hardness. This transformation plasticity accommodates strain,

Table 5
Average flexural strength values and standard deviation for ZSW and ZSZ samples, along with the corresponding sintering parameters.

SPS-protocol (°C/MPa/min)	Sample name	σ_f Average (MPa)	σ_f Standard deviation (MPa)	Sample name	σ_f Average (MPa)	σ_f Standard deviation (MPa)
1950/50/15	**ZSW.1**	407	52	**ZSZ.1**	343	127
2050/50/15	**ZSW.2**	384	57	**ZSZ.2**	317	13
2000/65/15	**ZSW.3**	490	42	**ZSZ.3**	476	71
2050/65/15	**ZSW.4**	461	37	**ZSZ.4**	434	49
2100/65/15	**ZSW.5**	407	59	**ZSZ.5**	423	21
2000/65/60	**ZSW.6**	516	49	**ZSZ.6**	447	58
2100/65/60	**ZSW.7**	497	43	**ZSZ.7**	431	112

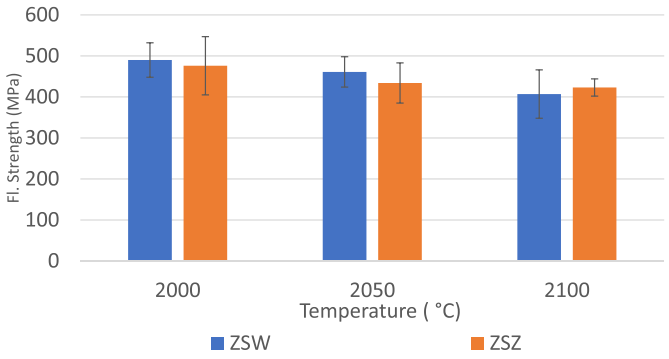

Fig. 14. Comparison of flexural strength between samples fabricated using high-energy WC milling and regular ZrO_2 milling, evaluated at 65 MPa and a dwell time of 15 min across different temperatures.

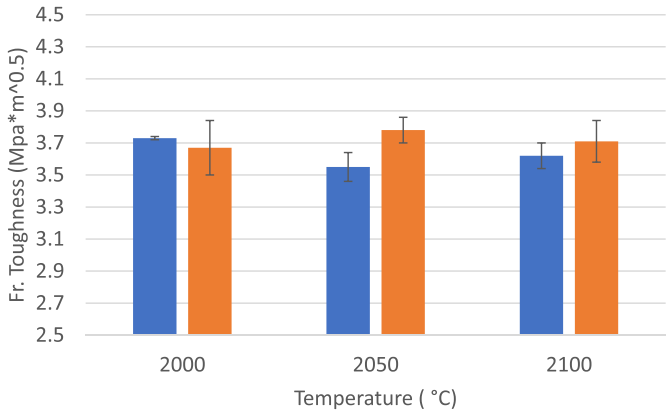

Fig. 15. Comparison of fracture toughness between samples fabricated using high-energy WC milling and regular ZrO_2 milling, evaluated at 65 MPa and a dwell time of 15 min across different temperatures.

increasing crack initiation resistance and slowing crack propagation [26].

Fig. 14 shows that the flexural strength values of the ZSW and ZSZ samples ranged between 384–516 MPa and 314–476 MPa, respectively. Interestingly, ZSW samples exhibited higher flexural strength in several cases, particularly at higher sintering temperatures and pressures, which is likely due to the increased ZrO_2 transformation toughening effect. The highest flexural strength was recorded for ZSW.6 (516 MPa), sintered at 2000 °C, 65 MPa, and a dwell time of 60 min, whereas the corresponding ZSZ.6 sample exhibited a lower strength of 447 MPa. This notable difference highlights the effectiveness of the ZrO_2 toughening mechanism in the ZSW samples under specific sintering conditions.

The flexural strength values obtained in this study align with previously reported results. Stadelmann et al. [10] reported flexural strength values of 329–558 MPa for ZrB_2-SiC composites sintered under similar conditions. Seetala et al. [11] found that flexural strength increased with longer milling times, reporting 426 MPa after 48 h of ball milling, while shorter milling durations (24 h) resulted in lower values of approximately 230 MPa. Hassan and Balani [3] observed an average flexural strength of 478 MPa for ZrB_2-20 vol% SiC composites sintered at 1950 °C. The consistency of the ZSW and ZSZ flexural strength values with literature data validates the reliability of the sintering protocols and mechanical testing methods used in this study.

3.3.3. *Fracture toughness*

The fracture toughness of the sintered ZrB_2-SiC composites was measured to assess the material's resistance to crack propagation, as well as its toughening mechanisms, with a focus on how different milling methods and sintering parameters, such as temperature, impact its toughness. This property is crucial for assessing the mechanical reliability of the composites, particularly for applications involving high thermal and mechanical loads, such as in aerospace and defense systems. In this study, Vickers indentation tests were performed on all the samples for the estimation of the fracture toughness (K_{IC}). The results, including the average values and standard deviations, are presented in Table 6 and illustrated in Fig. 15.

The ZSZ samples, which are characterized by their finer grain structure and the absence of the secondary ZrO_2 phase, generally exhibit higher fracture toughness than the ZSW samples. This is because the smaller grains contribute to an increased number of grain boundaries, which act as obstacles to crack propagation, thereby enhancing the material's resistance to fracture. In contrast, the ZSW samples contain larger grains and the secondary ZrO_2 phase, which reduces their toughness. Some of the toughening mechanisms observed in the materials from the current study included crack branching, crack deflection, crack bridging, and the fracture of SiC particles, consistent with findings reported in the literature [27]. During crack propagation, the cracks split into multiple smaller branches (crack branching). This phenomenon increases the surface area of the crack, thereby dissipating more energy and reducing the overall crack growth rate. The interaction of propagating cracks with grain boundaries or secondary phases causes the crack path to deviate (crack deflection). This deflection increases the crack length and reduces the driving force for propagation, thereby enhancing toughness. Microstructural features such as unfractured particles or fibers can bridge the crack faces, resisting their separation and improving toughness (crack bridging).

The SiC reinforcement particles act as toughening agents by fracturing or debonding during crack propagation, absorbing energy and slowing down crack growth (fracture of SiC particles). These mechanisms, combined with the finer grain size in ZSZ samples, result in improved fracture resistance compared to ZSW samples.

From Table 6 and Fig. 15, it can be observed that the fracture toughness values of the ZSW and ZSZ samples ranged between 3.51 and 3.76 MPa $m^{1/2}$ and 3.48–3.97 MPa $m^{1/2}$, respectively. Notably, the ZSZ samples consistently demonstrated slightly higher K_{IC} values, with the ZSZ.1 sample showing the highest toughness of 3.97 MPa $m^{1/2}$. In comparison, the corresponding ZSW.1 sample exhibited a lower toughness of 3.71 MPa $m^{1/2}$. The difference in toughness between the ZSZ and ZSW samples can be attributed to the absence of the secondary ZrO_2 phase and the finer grain size in the ZSZ samples. The smaller grains create more grain boundaries, which impede crack propagation, thereby enhancing the material's resistance to fracture.

Table 6
Average fracture toughness values and standard deviation for ZSW and ZSZ samples, along with the corresponding sintering parameters.

SPS-protocol (°C/MPa/min)	Sample name	K_{IC} Average (MPa·$m^{1/2}$)	K_{IC} Standard deviation (MPa·$m^{1/2}$)	Sample name	K_{IC} Average (MPa·$m^{1/2}$)	K_{IC} Standard deviation (MPa·$m^{1/2}$)
1950/50/15	**ZSW.1**	3.71	0.12	**ZSZ.1**	3.97	0.02
2050/50/15	**ZSW.2**	3.58	0.07	**ZSZ.2**	3.48	0.06
2000/65/15	**ZSW.3**	3.76	0.01	**ZSZ.3**	3.67	0.17
2050/65/15	**ZSW.4**	3.55	0.09	**ZSZ.4**	3.78	0.08
2100/65/15	**ZSW.5**	3.62	0.08	**ZSZ.5**	3.71	0.13
2000/65/60	**ZSW.6**	3.75	0.05	**ZSZ.6**	3.72	0.10
2100/65/60	**ZSW.7**	3.51	0.07	**ZSZ.7**	3.62	0.08

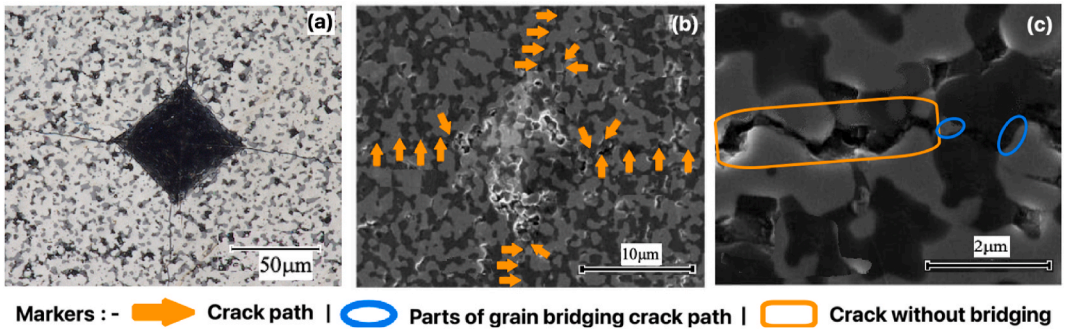

Fig. 16. Fracture surface features of ZSZ.1 showing (a) indentation with radial cracks, (b) crack deflection at grain boundaries, and (c) grain bridging and intergranular fracture at higher magnification.

The fracture toughness values obtained in this study are consistent with those reported in previous studies. Yuan et al. [18] observed fracture toughness values of 3.18 MPa $m^{1}/^{2}$ for ZrB_2-SiC composites prepared by high-energy ball milling and spark plasma sintering. Guo et al. [9] presented an average K_{IC} of 3.5 MPa $m^{1}/^{2}$ for ZrB_2-20 vol% SiC composites, sintered at 1800 °C under vacuum. Stadelmann et al. [10] reported K_{IC} values of 2.7–3.1 MPa $m^{1}/^{2}$ for ZrB_2-SiC composites sintered under similar conditions. The fracture toughness values measured in this study are thus in good agreement with the literature data, further validating the effectiveness of the sintering protocols and mechanical testing methods used.

3.3.4. *Fracture behavior and crack propagation mechanisms*

To provide further insight into the mechanisms contributing to the mechanical performance of the ZrB_2–SiC composites, surface SEM imaging was performed on a single representative ZSZ sample (ZSZ.1) that exhibited superior hardness and fracture toughness. Fig. 16 presents three sub-images taken at increasing magnifications: (a) shows a Vickers indentation imprint with visible radial cracks at 50 μm scale; (b) highlights crack path propagation at 10 μm scale, illustrating deflection at grain boundaries; and (c) provides a detailed view at 2 μm scale, clearly revealing grain bridging events and regions of intergranular fracture. Annotations indicate bridging grains (blue ellipses), crack propagation paths (orange arrows), and unbridged crack segments (orange outline).

Although derived from one sample only, these observations are consistent with the dominant toughening mechanisms proposed earlier in the manuscript. The fine-grained microstructure and clean ZrB_2–SiC interfaces in ZSZ samples promote crack deflection and bridging, which enhance fracture toughness and resistance to localized damage. In contrast, the ZSW samples, which exhibit coarser grains and contain minor ZrO_2 phases, are more susceptible to unbridged intergranular cracking and reduced crack resistance under indentation. Furthermore, the absence of secondary oxide phases in ZSZ likely results in lower residual stress concentrations at interfaces, leading to more controlled crack growth behavior. These qualitative observations support the earlier findings and reinforce the importance of grain size and phase purity in optimizing mechanical properties in SPS-processed ZrB_2–SiC composites.

3.4. *Oxidation resistance considerations*

Although direct oxidation testing was not performed in this study, a qualitative assessment based on microstructure and phase composition provides useful insights into the potential oxidation resistance of the sintered ZrB_2–SiC composites, which is a critical property for aerospace applications. The addition of 20 vol% SiC is widely recognized for enhancing oxidation resistance by forming a protective silica-based glass layer at elevated temperatures, which retards oxygen diffusion into the bulk ZrB_2 matrix [28]. Furthermore, recent investigations have confirmed that the synergy between SiC and fine ZrB_2 grains can promote the formation of a more continuous and stable borosilicate glass scale, improving the thermal stability and long-term oxidation behavior [29].

In this study, WC-milled (ZSW) samples exhibited 1–4 wt% monoclinic ZrO_2 as a secondary phase, likely introduced via abrasion from the milling media. Although this phase may contribute to densification, its presence can also influence the oxidation response. Prior studies suggest that secondary oxide phases such as ZrO_2 may compromise the integrity of protective surface scales by altering diffusion pathways or promoting localized stress development during thermal cycling [30]. In contrast, ZrO_2-milled (ZSZ) samples were free from ZrO_2 contamination and demonstrated finer grain structures and higher hardness, both of which correlate with reduced porosity and enhanced oxidation resistance due to more uniform and adherent oxide layer formation [31]. While no experimental oxidation data are presented herein, the observed microstructural features and phase compositions suggest that ZSZ samples may offer better oxidation resistance than ZSW samples. These interpretations align with reported trends in the literature and will guide future work, which will include isothermal and cyclic oxidation testing to validate these projections quantitatively.

4. Conclusions

The study demonstrated that high-energy WC milling significantly improves the densification and flexural strength of ZrB_2-SiC composites compared to conventional ZrO_2 milling. While ZSZ samples exhibited higher hardness and fracture toughness, the ZSW samples displayed superior flexural strength, attributed to the ZrO_2 phase transformation toughening mechanism. The following conclusions can be drawn.

- Enhanced densification was observed in ZSW samples, achieving a maximum relative density of 99.2 % at 2100 °C, 65 MPa, for 15 min, compared to 96.5 % for ZSZ samples under the same conditions. This improved densification in ZSW is due to WC milling's sintering aid effect, which promotes grain boundary diffusion and particle packing.
- XRD analysis revealed secondary ZrO_2 phases in ZSW samples, caused by abrasion and local oxidation during WC milling. In contrast, ZSZ samples remained phase-pure, benefiting from the stability of ZrO_2 milling balls.
- ZSZ samples exhibited consistently higher hardness, peaking at 17.38 GPa (ZSZ.1), compared to 14.33 GPa for ZSW samples (ZSW.1). The finer grain size in ZSZ samples contributed to their superior hardness, while softer ZrO_2 phases reduced the hardness of ZSW.
- ZSZ samples demonstrated higher fracture toughness (up to 3.97 MPa $m^{1}/^{2}$) due to finer grains and the absence of secondary phases. Despite lower toughness, ZSW samples displayed higher flexural strength (up to 516 MPa), driven by ZrO_2 transformation toughening, which absorbs energy during bending stresses. This

toughening effect was not observed in fracture toughness measurements, as Vickers indentation does not induce sufficient stress for phase transformation.
- The results align with previous studies, where flexural strengths of 333–584 MPa and toughness values of 3.4–4.1 MPa $m^{1}/^{2}$ were reported for ZrB_2-SiC composites under similar conditions.

CRediT authorship contribution statement

Iason Krinis: Validation, Investigation, Conceptualization, Methodology, Data curation, Writing – review & editing. **Prakhar Jindal:** Visualization, Methodology, Funding acquisition, Conceptualization, Writing – review & editing, Supervision, Investigation, Data curation, Writing – original draft. **Vera Popovich:** Supervision, Project administration, Writing – review & editing, Resources. **Hans Brouwer:** Methodology, Resources. **Jyoti Botchu:** Supervision, Writing – review & editing. **Yinglu Tang:** Supervision, Validation.

Declaration of competing interest

The authors declare the following financial interests/personal relationships which may be considered as potential competing interests: Prakhar Jindal reports financial support was provided by European Union. Prakhar Jindal reports financial support was provided by Horizon Europe. If there are other authors, they declare that they have no known competing financial interests or personal relationships that could have appeared to influence the work reported in this paper.

Acknowledgement

This work is supported by Horizon Europe's research and innovation programme under the Marie Sklodowska-Curie grant agreement No. 101107214. The authors acknowledge the extensive support received from the Materials Science and Engineering section of the Faculty of Mechanical Engineering and Space System Engineering section of the Faculty of Aerospace Engineering, Delft University of Technology, Netherlands. Mr. Richard Huizenga, at the Department of Materials Science and Engineering of the Delft University of Technology, is acknowledged for the X-ray analysis.

APPENDIX - A. :

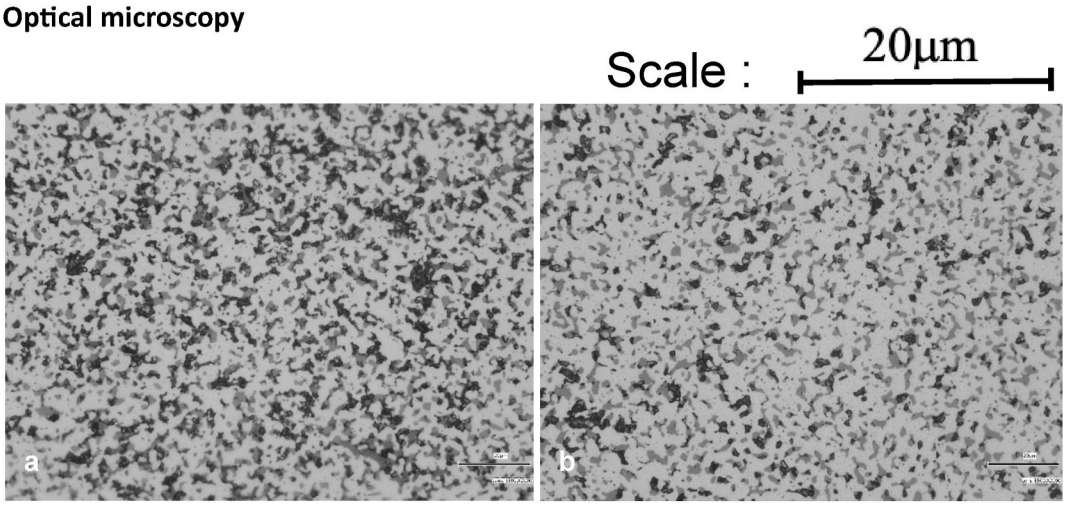

Fig. 1. Microstructures of samples a) ZSW.1 and b) ZSZ.1 (x 2000).

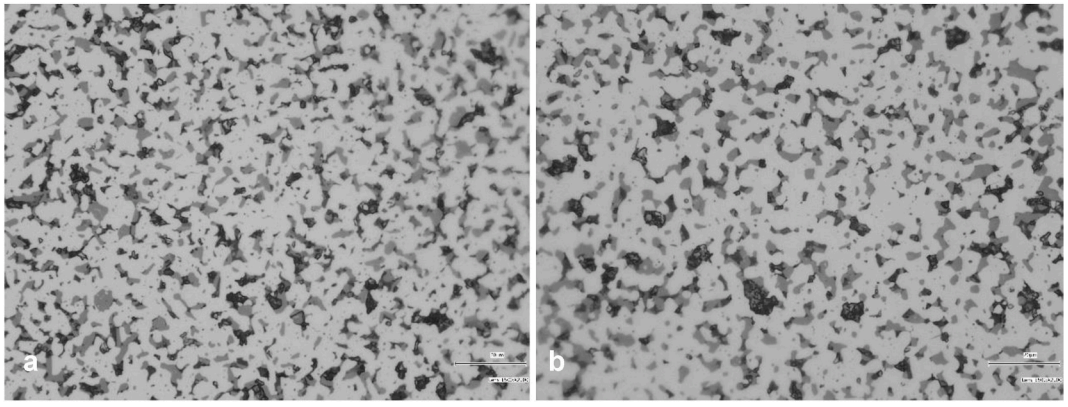

Fig. 2. Microstructures of samples a) ZSW.2 and b) ZSZ.2 (x 2000).

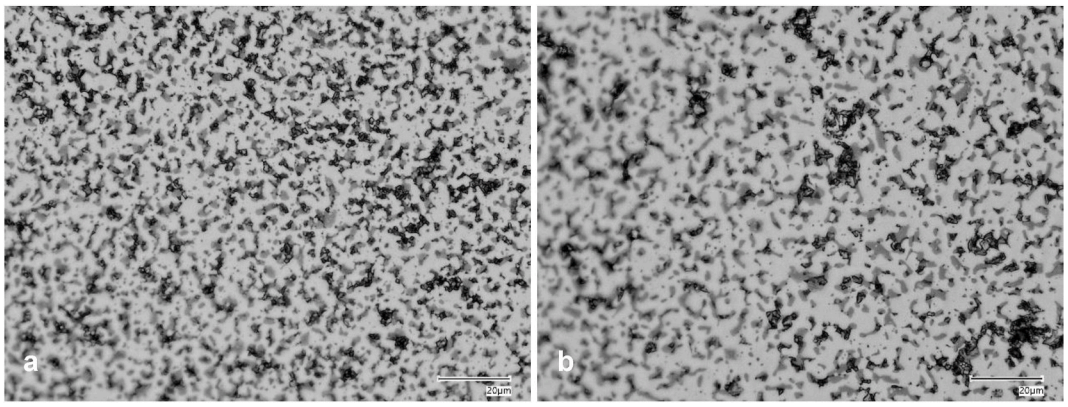

Fig. 3. Microstructures of samples a) ZSW.3 and b) ZSZ.3 (x 2000).

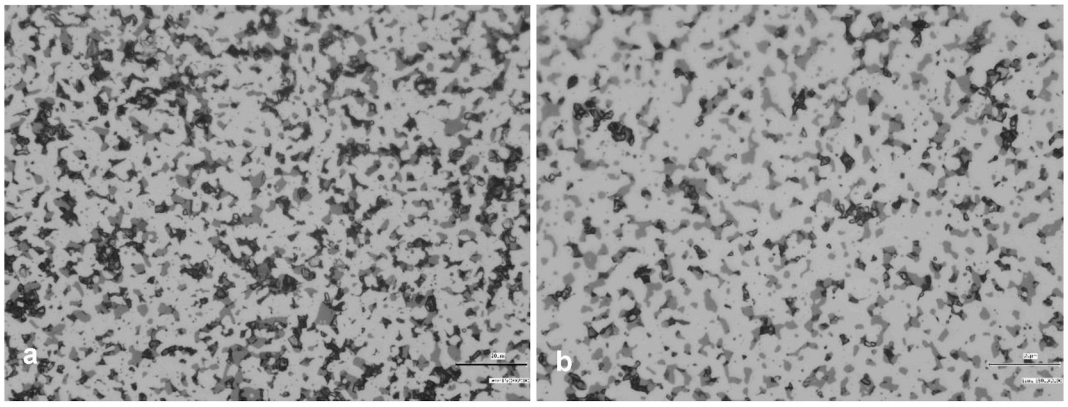

Fig. 4. Microstructures of samples a) ZSW.4 and b) ZSZ.4 (x 2000).

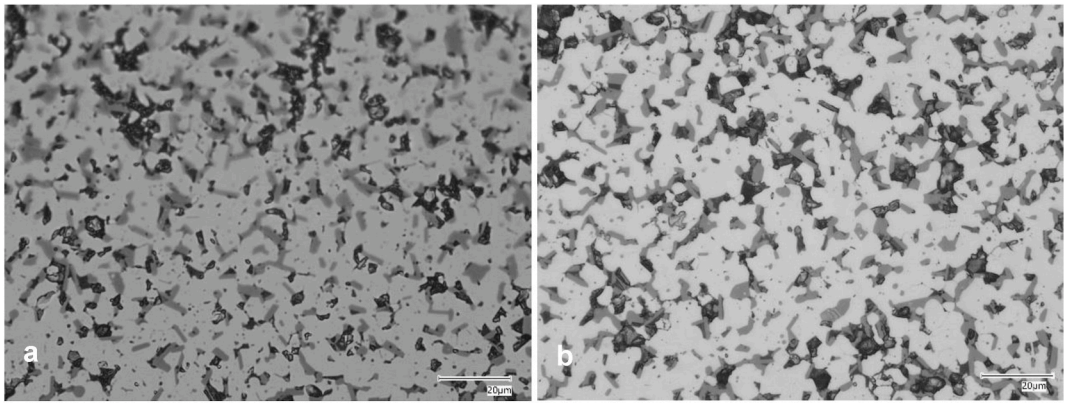

Fig. 5. Microstructures of samples a) ZSW.5 and b) ZSZ.5 (x 2000).

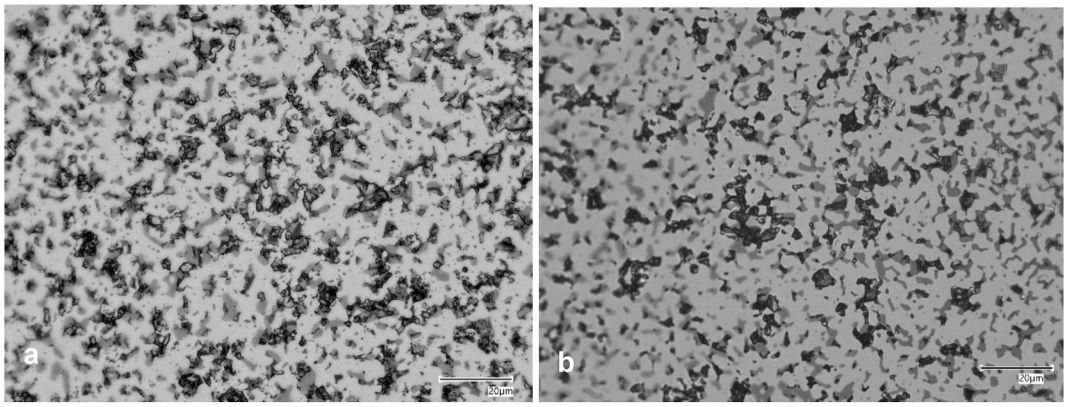

Fig. 6. Microstructures of samples a) ZSW.6 and b) ZSZ.6 (x 2000).

References

[1] D. Sciti, A. Vinci, L. Zoli, P. Galizia, S. Failla, S. Mungiguerra, G.D. Di Martino, A. Cecere, R. Savino, Propulsion tests on ultra-high-temperature ceramic matrix composites for reusable rocket nozzles, J. Adv. Ceram. 12 (2023) 1345–1360, https://doi.org/10.26599/JAC.2023.9220759.

[2] A. Naughton-Duszova, E. Bączek, M. Podsiadło, Selected properties of ZrB2 composites obtained by SPS method for parts of electro-erosion shaping machines, Mechanik (2018) 155–158, https://doi.org/10.17814/mechanik.2018.2.32.

[3] R. Hassan, K. Balani, Densification mechanism of spark plasma sintered ZrB2 and ZrB2-SiC ceramic composites, Mater Charact 179 (2021) 111320, https://doi.org/10.1016/j.matchar.2021.111320.

[4] M.S. Asl, Z. Balak, Fabrication and characterization of ZrB2 ceramic in presence of graphite platelet and SiC, Silicon 15 (2023) 6911–6919, https://doi.org/10.1007/S12633-023-02553-W/METRICS.

[5] J.J. Swab, J. Jarman, W. Fahrenholtz, J. Watts, Mechanical properties of ZrB2 ceramics determined by two laboratories, Int. J. Appl. Ceram. Technol. 20 (2023) 3097–3103, https://doi.org/10.1111/IJAC.14429;JOURNAL:JOURNAL:17447402;REQUESTEDJOURNAL:JOURNAL:17447402;WGROUP:STRING:PUBLICATION.

[6] E. Zapata-Solvas, D.D. Jayaseelan, H.T. Lin, P. Brown, W.E. Lee, Mechanical properties of ZrB2- and HfB2-based ultra-high temperature ceramics fabricated by spark plasma sintering, J. Eur. Ceram. Soc. 33 (2013) 1373–1386, https://doi.org/10.1016/J.JEURCERAMSOC.2012.12.009.

[7] D. Ni, Y. Cheng, J. Zhang, J.X. Liu, J. Zou, B. Chen, H. Wu, H. Li, S. Dong, J. Han, X. Zhang, Q. Fu, G.J. Zhang, Advances in ultra-high temperature ceramics, composites, and coatings, J. Adv. Ceram. 11 (1) (2021) 1–56, https://doi.org/10.1007/S40145-021-0550-6, 11 (2021.

[8] S.Q. Guo, Densification of ZrB2-based composites and their mechanical and physical properties: a review, J. Eur. Ceram. Soc. 29 (2009) 995–1011, https://doi.org/10.1016/J.JEURCERAMSOC.2008.11.008.

[9] Q. Guo, J. Li, Q. Shen, L. Zhang, Effect of high-energy ball milling of ZrB2 powder on the microstructure and mechanical properties of ZrB2-SiC ceramics, Key Eng. Mater. (2012) 512–515, https://doi.org/10.4028/WWW.SCIENTIFIC.NET/KEM.512-515.723, 723–728.

[10] R. Stadelmann, Mechanical Properties and Thermal Residual Stresses of ZrB2-SiC Ceramic Composites for Hypersonic Vehicle Applications, 2013.

[11] N. Seetala, C.L. Prevo, L.E. Matson, T.S. Key, I.I. Park, Spark plasma sintering of high-energy ball-milled ZrB2 and HfB2 powders with 20vol% SiC, Mater. Sci. Forum 941 (2018) 1990–1995. https://doi.org/10.4028/www.scientific.net/MSF.941.1990.

[12] C.B. Ponton, R.D. Rawlings, Vickers indentation fracture toughness test part 1 review of literature and formulation of standardised indentation toughness equations, Mater. Sci. Technol. 5 (1989) 865–872, https://doi.org/10.1179/mst.1989.5.9.865.

[13] B.R. Lawn, M.V. Swain, Microfracture beneath point indentations in brittle solids, J. Mater. Sci. 10 (1975) 113–122, https://doi.org/10.1007/BF00541038.

[14] G.D. Quinn, R.C. Bradt, On the vickers indentation fracture toughness test, J. Am. Ceram. Soc. 90 (2007) 673–680, https://doi.org/10.1111/j.1551-2916.2006.01482.x.

[15] H. Fischer, Fracture toughness of dental ceramics: comparison of bending and indentation method, Dent. Mater. 18 (2002) 12–19, https://doi.org/10.1016/S0109-5641(01)00005-7.

[16] E.A. Lantsev, A.V. Nokhrin, M.S. Boldin, K.E. Smetanina, Y.V. Blagoveshchenskii, N.V. Isaeva, A.A. Murashov, V.N. Chuvil'deev, A.V. Terent'ev, N.Y. Tabachkova, Preparation of ultrafine-grained WC–ZrO2 ceramics by spark plasma sintering, Inorg. Mater. 59 (2023) 537–543, https://doi.org/10.1134/S0020168523050114/METRICS.

[17] A.L. Chamberlain, W.G. Fahrenholtz, G.E. Hilmas, D.T. Ellerby, High-strength zirconium diboride-based ceramics, J. Am. Ceram. Soc. 87 (2004) 1170–1172.

[18] J.-H. Yuan, Q.-Y. Liu, Y. You, L.-Y. Zeng, M.-W. Bai, L.R. Blackburn, W.-M. Guo, H.-T. Lin, Effect of ZrB2 powders on densification, microstructure, mechanical properties and thermal conductivity of ZrB2-SiC ceramics, Ceram. Int. 47 (2021) 15843–15848, https://doi.org/10.1016/j.ceramint.2021.02.158.

[19] Z. Zhang, H. Yi, M. Liang, L. Xie, B. Yin, Y. Yang, Effect of sintering process on microstructure and properties of (Zr0.2Ta0.2Ti0.2Cr0.2Hf0.2)Si2 high-entropy silicide ceramics, Coatings 14 (2024) 1280, https://doi.org/10.3390/COATINGS14101280, 1280 14 (2024.

[20] A. Leriche, F. Cambier, S. Hampshire, Sintering of ceramics, Reference Module in Materials Science and Materials Engineering (2017), https://doi.org/10.1016/B978-0-12-803581-8.10288-7.

[21] Properties: Zirconia - ZrO2, Zirconium dioxide, (n.d.). https://www.azom.com/properties.aspx?ArticleID=133 (accessed May 30, 2025).

[22] ZrO2, (n.d.). https://www.globalsino.com/EM/page2070.html (accessed May 30, 2025).

[23] Properties: sintered silicon carbide (SiC) properties and applications, (n.d.). https://www.azom.com/properties.aspx?ArticleID=15 (accessed May 30, 2025).

[24] M.J. Gasch, D.T. Ellerby, S.M. Johnson, Ultra high temperature ceramic composites, handbook of ceramic composites, 197–224, https://doi.org/10.1007/0-387-23986-3_9, 2005.

[25] B. Pathak, B. Maskey, A. Bhochhibhoya, D. Devkota, Transformation-toughened zirconia: an overview, J. Nepalese Prosthodontic Soc. 5 (2022) 19–24, https://doi.org/10.3126/JNPROSSOC.V5I1.53394.

[26] R.H.J. Hannink, P.M. Kelly, B.C. Muddle, Transformation toughening in zirconia-containing ceramics, J. Am. Ceram. Soc. 83 (2000) 461–487, https://doi.org/10.1111/J.1151-2916.2000.TB01221.X;WGROUP:STRING:PUBLICATION.

[27] M.S. Asl, M.G. Kakroudi, S. Noori, Hardness and toughness of hot pressed ZrB2–SiC composites consolidated under relatively low pressure, J. Alloys Compd. 619 (2015) 481–487, https://doi.org/10.1016/J.JALLCOM.2014.09.006.

[28] T.G. Aguirre, B.W. Lamm, C.L. Cramer, D.J. Mitchell, Zirconium-diboride silicon-carbide composites: a review, Ceram. Int. 48 (2022) 7344–7361, https://doi.org/10.1016/J.CERAMINT.2021.11.314.

[29] L. Li, Y. Yu, J. Yang, C. Cheng, W. Duan, C. Ma, A ZrB2-SiC(Al) coating with improved oxidation resistance for C/C composites: design, experimental verification and oxidation mechanism, J. Eur. Ceram. Soc. 44 (2024) 3487–3500, https://doi.org/10.1016/J.JEURCERAMSOC.2024.01.067.

[30] Y. Yu, L. Li, C. Ma, C. Cheng, J. Ren, Oxidation resistance, oxidation mechanism and mechanical properties of ZrB2-SiC-TaB2 ceramics, Ceram. Int. 51 (2025) 13522–13536, https://doi.org/10.1016/J.CERAMINT.2025.01.195.

[31] L. Zhao, C. Hou, X. Jin, P. Li, Z. Wang, X. Fan, Oxidation behaviors of ZrB2–SiC ceramics with different porosity, Adv. Eng. Mater. 25 (2023) 2201313, https://doi.org/10.1002/ADEM.202201313.